Porous Liquids Responsive to Light

Manish Kumar Dinker
Nanjing Tech University
Kan Zhao
Nanjing Tech University
Zhengxing Dai
Nanjing Tech University
Lifeng Ding
Xi'an Jiaotong-Liverpool University
Xiao-Qin Liu
Nanjing Tech University
Lin-Bing Sun (lbsun@njtech.edu.cn)
Nanjing Tech University https://orcid.org/0000-0002-6395-312X

Article

Keywords:

Posted Date: August 16th, 2022

DOI: https://doi.org/10.21203/rs.3.rs-1430877/v1

Abstract

Porous liquid is a unique liquid medium that combines permanent porosity of porous solid with the fluidity of liquid, and this special characteristic makes it potential in various applications. Here we report the first photoresponsive porous ionic liquid (PPIL) by solubilizing photoresponsive metal-organic polyhedron (PMOP, constructed from dicopper and azobenzene-containing carboxylate) in polyethylene-glycol-functionalized bulky ionic liquid (IL). Owing to favorable ion interactions, bulky IL molecules encircle outside PMOP cages, and the inter cavities are maintained. The azobenzene moieties can be isomerized freely in the obtained PPILs to expose and shelter active sites upon visible and UV light irradiations. Hence, the adsorption capacity of PPILs is controllable by light irradiation, and the change in CO_2 uptake is up to 30% which is different from neat IL with negligible change. This study might inspire the development of new adsorption process regulated by light instead of conventional pressure and temperature swing adsorption technologies.

Full Text

Porous liquids have drawn increasing attention owing to the combination of porous solid and fluid which furnishes resulting flowing system eternal porosity.[1-4] The permanent pores endow fluids with subsidiary physicochemical properties, rendering as suitable solitary media for a variety of applications like adsorption and catalysis.[5-7] Intrinsic cavities in fluidic systems can be generated by three methods, that is, porous hosts' functionalization (type I) as well as their solubilization (type II) or dispersion (type III) in relatively size-excluded solvents.[8-10] In present, basic entities for rigid host structures are mostly from metal-organic frameworks, porous organic cages and zeolites, while chlorinated solvents and ionic liquids (ILs) are chosen as sterically hindered solvents.[11-15] Such combinations lead to the formation of a series of interesting porous liquids.

Life systems are capable of modulating themselves to variable environments for survival. Inspiring by this, smart materials that can respond to external stimuli (e.g. temperature, light, and pH) with tunable features have been developed.[16-20] Among various external stimuli, light attracts great interest since it allows rapid and precise control with rare undesirable byproducts.[21-24] Azobenzene is a classic photoresponsive molecule, its configuration transformation between *cis* and *trans* isomer can be induced by ultraviolet (UV) and visible light irradiation.[25-27] On the basis of such configuration transformation, it is promising to construct azobenzene-based materials with tunable performance through sheltering and exposing active sites.[28-32] By introducing photoresponsive porous moieties to bulky liquids, it is expected to endow the fluids with properties responsive to light. As a result, the adsorption process is possible to run by light irradiation, which is remotely controllable and much more energy-efficient in comparison with traditional pressure and temperature swing. Albeit intriguing, the fabrication of photoresponsive porous liquids has never been reported.

Here, we report the first example of photoresponsive porous ionic liquid (PPIL) by dissolving a photoresponsive metal-organic polyhedron (PMOP, constructed from the coordination of dicopper and azo-containing carboxylate) in a newly designed size-excluded ionic liquid [IL(NTf_2), alkylated polyethylene glycol (PEG)-linked bis(imidazoliumbutyl) di(trifluoromethanesulfonyl)amide]. By controlling the content of PMOP, type II porous liquid is successfully created. The results reveal the structural integrity of PMOP in IL(NTf_2) and bulky IL molecules encircling outside the cages due to favorable ion interactions, thus the inter cavities are maintained. The azobenzene moieties in PPIL can transform between *trans* and *cis* isomerization reversibly upon UV and visible light irradiation. Hence, the PPIL upon visible light irradiation whose active sites are exposed can capture more CO_2 than its counterpart upon UV light irradiation with sheltered active sites. Remarkably, after *trans*/*cis* isomerization, the PPIL exhibits the change in CO_2 uptake up to 30%, which is obviously superior to neat IL with negligible change. Moreover, the present PPIL remains intact after one year and the photoresponsive adsorption capacity is well preserved.

Results

Fabrication and characterization of the PPILs

The PPILs were fabricated by solubilizing PMOP in size-excluded IL. PMOP, [$Cu_{24}(C_{16}H_{12}N_2O_4)_{24}$)], with a cuboctahedral conformation was obtained by the crystallization of $Cu(OAc)_2$ and organic linker 5-((2,4-dimethylphenyl)diazenyl)isophthalic acid possessing 120° angle (Supplementary Fig. 1). With permanent pore size (14 Å) and cavity (21.4 Å), PMOP changed its diameter from 40.4 to 31.1 Å after *trans*-to-*cis* isomerization owing to the readily twisted pendant azobenzene units under UV light irradiation (Supplementary Fig. 2).[33] Apart from examining the obtained cage based on the series of analytical results to validate its molecular integrity (Supplementary Figs. 3–5), the isomerization was confirmed by analyzing dispersed cages in ethanol upon light irradiations (Supplementary Fig. 6). Besides, optical response of solid PMOP under UV and visible light irradiation was found almost scant owing to the aggregation in bulk, which is in consistent with previous reports.[34]

The PEG-containing long-chain IL, IL(NTf_2), with molecular dimension of 37.5 x 18.6 x 14.1 $Å^3$ was pre-designed, and used as sterically hindered solvent for PMOP (Fig. 1a and Supplementary Fig. 7). Other properties, especially low viscosity, high thermal stability (discussed later), and diverse functionality of IL(NTf_2) could be considered as ideal inherent features to provide favorable conditions. Hence, 2% of PMOP was dispersed initially in IL(NTf_2) to obtain a parent solution (Supplementary Fig. 8). Later, parent solution was diluted successively with IL(NTf_2) having innate yellow imbue to prepare lucid type II PPILs with PMOP contents of 0.05%, 0.1% and 0.2% (Supplementary Fig. 9). In contrast to neat IL, ^1H nuclear magnetic resonance (NMR) spectra obtained of these PPILs illustrate shifts (δ) in the peaks belonging to the protons of IL(NTf_2) (Fig. 1b and Supplementary Fig. 10). Such downshifts are caused by the magnetic susceptibility and the paramagnetism of copper-based complexes which is observed by adding

$Cu(OAc)_2$ (3%) in the neat IL and obtaining ^1H NMR spectrum (Fig. 1a). These downward shifts due to the presence of Cu(II) salt in IL confirms the availability of PMOP (containing Cu) in IL(NTf_2). This trend of downshifts continues with the increase of PMOP contents (0.05–0.2%) in IL(NTf_2) (Fig. 1a and Supplementary Fig. 10). Meanwhile, these shifts (δ) also indicate the probable interaction of IL molecules [both anionic, NTf_2^- and cationic, $(PEG\text{-}bis\text{-}Im_2)^{2+}$ moieties] with the cage periphery. Fourier transform infrared (FTIR) spectra of IL depict absorption peaks at 1348 and 1195 cm^{-1} [belonging to v(C–N) and v(C–O) of imidazolium and PEG chain part] which get broaden after adding PMOP (Supplementary Fig. 11). Such phenomenon confirms the interaction between IL moieties and the cage.

The presence of PMOP with various contents in IL was further observed by thermogravimetric (TG) analyses. The PPILs show slight enhancement in the thermal stability (> 300 °C) than neat IL(NTf_2) (Supplementary Figs. 12 and 13). Besides, X-ray diffraction (XRD) patterns of PPILs indicate the existence of PMOP. Apparently, the XRD peak at 12.5° which belongs to the crystalline PMOP,[33] can also be seen in PPILs, and found abating gradually with the decrease in MOP content from 2 to 0.05% in IL (Supplementary Fig. 14). These results provide tangible evidence about the availability and stability of PMOP in IL(NTf_2). Viscosity and density measurements of the obtained PPILs reveal minor decrements in the viscosities and densities after dissolving PMOP (0.05 – 0.2%) in IL(NTf_2) (Supplementary Fig. 15 and Supplementary Table 1). This can be attributed to the additional free volume/cavity created by cages into the IL which alters the fluidic nature of the resulting liquids.[35] The PEG chain, as a potential solubilizer for many complex organic compounds in various ILs,[36,37] therefore plays an important role here to solubilize PMOP in IL(NTf_2).

To gain a molecular-level understanding of solvent's size-exclusion as per the pore-sizes of both isomerized cages, molecular dynamic simulations were implemented.[38] As shown in Fig. 1c, IL(NTf_2) does not occupy the inter cavity but surround both the cages outside backbones. Also, the bulk $(PEG\text{-}400\ bis\text{-}Im_2)^{2+}$ chain truncates itself around the *trans*-PMOP on the two N-heterocyclic sites carrying positive charges, which tends to point outside the periphery (Fig. 1c and Supplementary Video 1). As for NTf_2^-, affected by favorable electrostatic interaction with the cations, the anions are stuck around the vicinity between the *trans*-PMOP and the $(PEG\text{-}400\ bis\text{-}Im_2)^{2+}$ chain instead of entering inside. A similar dynamic manner could be observed for the *cis*-MOP as well (Fig. 1d and Supplementary Video 2). The above findings are further validated by the radial distribution functions (Fig. 2), where the distribution of IL(NTf_2) (both cations and anions) only exist beyond the inter cavity sphere diameter (dash line). It is worth noticing that, compared with *trans*-PMOP, the existence of IL leads to a slight reduction in pore size distribution in the *cis*-MOP while the dominant pore size is still maintained (Fig. 2). We envisage that though IL molecules do not enter the *cis*-PMOP cavities, some cavity windows are blocked due to the bending of pendant azobenzene groups. However, for both *trans*- and *cis*-PMOP in IL(NTf_2), the inter-cavity is still porous, endowing the entire system with permanent porosity.

Photoresponsive properties of the PPILs

In order to observe the photoresponsive behavior of the obtained PPILs, the samples were consecutively irradiated with UV and visible light. UV-Vis spectra obtained of PPIL-0.05%, 0.1% and 0.2% depict a rapid absorbance decrease and increase at 340 and 438 nm after 10–90 s of UV light irradiation, and the breakthrough is observed within 3 min (Fig. 3 and Supplementary Figs. 16–18). Such phenomenon is caused by π–π* and *n*–π* transitions of *trans*- and *cis*-isomer owing to the pendant azobenzene moieties on discrete PMOP in IL. Durability of *cis*-isomer was examined by maintaining UV-light (365 nm) irradiated PPIL in dark for 4 h, and the obtained UV-Vis spectra eventually justify its optical stability for prospective guest uptake-release (Supplementary Fig. 19). Besides, the absorbance at 340 nm was recovered after consecutive 3 min of visible light irradiation (450 nm) (Fig. 3b). Moreover, such *trans*/*cis* isomerization of PPILs (0.05–0.2%) was found completely reversible by switching UV- and visible light irradiation (Fig. 3c and Supplementary Figs. 20 and 21). These analytical results demonstrate better optical response of PMOP dissolved in IL(NTf_2) due to cage isolation than in bulk where they remain aggregated, as discussed in the previous part.

In the PPIL, configuration transformation from *cis* to *trans* azobenzene isomers can also be triggered by heat besides visible light irradiation. The heat response of the prepared PPILs was thus examined. After UV-light irradiation, the sample (*cis*-isomer) was treated at 60 °C for 10 and 20 min under dark, and the UV-Vis spectra were collected. The obtained spectra reveal the recovery of absorbance at 340 nm which clearly signifies the transformation of *cis*- to *trans*-isomer (Fig. 3d). Furthermore, the sample was cooled down to room temperature; and after UV-light irradiation, the obtained UV-Vis spectra eventually depict absorbance decrease at 340 nm again which confirms the reversible isomerization from *trans* to *cis*. Besides, such transformations after heating was physically observed by change in color of PPIL-0.2% from yellow to orange which regains its usual color after cooling down (Fig. 3d).

Photoresponsive adsorption behavior of the PPILs

CO_2 was chosen as a guest molecule to examine its interaction with the obtained PPILs. The PPILs depicted higher CO_2 uptakes both at low (Supplementary Fig. 22) and high pressures (Fig. 4) than neat IL(NTf_2), owing to the available intrinsic cavities. At low pressure (1 bar, 25 °C), PPIL-0.1% captured the highest amount of CO_2 among its counterparts, while PPIL-0.2% remained lowest due to probable mild aggregation of PMOP (0.2% in IL) which sterically hindered the active sites. To examine the photoresponsive adsorption behavior of PPILs, CO_2 adsorption was carried out upon visible (450 nm) and UV light (365 nm) irradiations. At 1 bar, PPIL-0.1% depicted 0.140 mmol g^{-1} of CO_2 uptake under visible light than upon UV light irradiation (0.127 mmol g^{-1}) (Supplementary Fig. 22). It signifies that 1 g of PMOP in IL captures 5.381 and 4.087 mmol of CO_2 i.e about 40 and 31 CO_2 molecules per cavity under visible and UV light irradiations. All the credit goes to the pendant azobenzene groups on the PMOP which under visible light remain stretched to expose active sites (*trans*-isomer) while under UV-light, they get twisted and block the active sites (*cis*-isomer). Although PPIL-0.05% depicted high CO_2 uptake (0.107 mmol g^{-1}) than neat IL (0.087 mmol g^{-1}) under visible light, its optical behavior (change in CO_2 uptake, %) upon UV-Vis light irradiation was inferior to PPIL-0.1% due to low content of PMOP (Supplementary

Fig. 22). Despite lowest CO_2 adsorption, PPIL-0.2% depicted highest change in CO_2 uptake under light irradiations owing to the lowest viscosity among PPILs which persuade its optical responsiveness at low pressure. Apparently, no optical behavior of neat IL for gas molecule was observed due to the absence of any photoresponsive moieties. Besides, PMOP in bulk was found optically weak, i.e. almost no change in CO_2 uptake under UV- and visible light irradiations which is caused by the aggregation of cages in solid state (Supplementary Fig. 23).

In order to examine the fate of PMOP in other ILs and the respective controlled CO_2 adsorption under light, PMOP solubilization was attempted in 1-butyl-3-methylimidazolium di(tifluoromethanesulfonyl)amide [(Bmim)(NTf_2)], *N*-butyl pyridinium di(tifluoromethanesulfonyl)amide [(Bpy)(NTf_2) and dodecyltributylphosphonium bromide [(DTP)(Br)]. Intriguingly, only (DTP)(Br), owing to its molecular size and long alkyl chains is found solubilizing 0.5% of PMOP to obtain type II PPIL, named PPBr-0.5% (Supplementary Fig. 24). Though the change in CO_2 uptake (%) under UV-Vis light by PPBr-0.5% was fairly higher (12.3%) than by PPIL-0.1% (8.2%) at 1 bar. Yet, the high content of PMOP in (DTP)(Br) found incompetent (probably due to aggregation) as the maximum CO_2 adsorption by PPBr-0.5% was found slightly lower in contrast of PPIL-0.1% (Supplementary Fig. 25). This justify PPIL-0.1% as an ideal contender for controlled CO_2 uptake under light, respectively. To further exemplify the optical dominance of PPIL-0.1%, selective gas separation (CO_2/N_2) under light was carried out. At 1 bar, no effect of N_2 was observed on the CO_2 adsorption by PPIL-0.1% while the capturing of N_2 molecules almost remain negligible with low change amount (%) under UV-Vis light (Supplementary Fig. 26). This indicates that the present materials may be potential active for the separation of CO_2 and N_2, which is demanded by carbon capture from flue gas.

The adsorptive analytical results at low pressure demonstrate that the obtained PPILs possess permanent porosity, and to observe their optimum photoresponsive adsorption behavior, high pressure is needed for such liquid mediums. Hence, gas adsorption using the PPILs at high pressure were further performed (Fig. 4). In general, the uptakes at high pressure of 10 bar are obviously higher than that at low pressure of 1 bar. IL with dissolved PMOP (0.1%) capture 0.87 mmol g^{-1} of CO_2 at 10 bar, while the adsorption capacity of PPIL-0.2% remains the lowest (0.58 mmol g^{-1}) (Supplementary Fig. 27). As discussed earlier, the high content of PMOP (0.2%) dissolved in IL probably causes its partial aggregation which affects the capability for gas uptake under light irradiations. This is exactly what is observed when the adsorption of CO_2 on PMOP in bulk (solid state) was carried out at 10 bar and depict optically weak behavior (change in uptake, only 2.2%) upon visible (450 nm) and UV light (365 nm) irradiations (Supplementary Fig. 28). The utmost photoresponsive behavior for CO_2 at high pressure was observed by PPIL-0.05% owing to absolute isolation of 0.05% PMOP in IL and thus, better optical activity upon light irradiation (Fig. 4a). The PPIL-0.05% shows the change in CO_2 uptake of 30%, whereas neat IL depicts negligible optical response to CO_2 at high pressure (Fig. 4b). Therefore, the results of high-pressure adsorption confirm the low-pressure experiments, evidencing the existence of intrinsic cavities of the resultant PPILs which are responsive to light.

Durability of the PPILs

To ensure the constancy of PPILs for a long period of time, 12 months old sample of PPIL-0.1% was characterized again. FTIR spectrum obtained of old PPIL-0.1% depicts similar absorption patterns as of the fresh one (Supplementary Fig. 29). Moreover, ^{1}H NMR spectra of 12 months old sample of PPIL-0.1% illustrates comparable downward shits (δ) in the peaks as of depicted by the fresh sample in contrast of neat IL(NTf_2) (Supplementary Fig. 30). These analyses evidently confirm the lastingness of the PPILs. Besides, in order to confirm the presence of cavity as well as the guest interaction of old sample upon light irradiations, CO_2 uptake was carried out again. The adsorption of CO_2 on the old sample under UV and visible lights has followed the similar trend as of the fresh PPIL-0.1% (Supplementary Fig. 31), thus substantiating the robustness of the PPILs for long duration.

Discussion

In conclusion, we have demonstrated the successful fabrication of the first porous liquid responsive to light by dissolving azo-functionalized PMOP in sterically hindered PEG-containing IL. The presence of permanent porosity in the obtained PPILs is verified by simulated and experimental results. Thanks to the peculiar chemistry of azobenzene moieties on the cage, they can be isomerized freely in PPILs to expose and shelter active sites upon light irradiation. As a result, the adsorption capacity of PPILs can be controlled by irradiation with UV or visible lights, which is different from neat IL with no change upon light irradiation. Traditionally, the adsorption capacity of adsorbents is controlled by pressure and temperature, and pressure swing adsorption and temperature swing adsorption processes are frequently used in industry. The present materials may open up an avenue for the development of new adsorption process regulated by light, which is remotely controllable and energy-efficient. In addition, the dissolution of cages in IL rather than dispersion prolongs the lifetime, and the PPILs are stable even after one year. The high thermal stability, long durability, and photoresponsive properties make the present PPILs promising for various applications.

Methods

Synthesis of the ligand

Ligand 5-((2,4-dimethylphenyl)diazenyl)isophthalic acid) was synthesized as per our earlier report.[33] Initially, 2,4-dimethylaniline solution (2.4 g, 20 mmol in 80 mL of DCM) was mixed with the solution of oxone (2.5 g, 40 mmol in 20 and 180 mL of DCM and water), and stirred in an open condition. The formation of nitroso-compound can be observed after 12 h when the solution turns eventually green. Next, the DCM layer was separated and washed with 1M HCl, twice. The product (2,4-dimethyl-1-nitrosobenzene) was obtained by drying the DCM solution in anhydruous $MgSO_4$, and finally DCM was removed by rota evaporation. Afterward, the product (0.81 g, 6 mmol) with dimethyl-5-aminoisophthalate (0.84 g, 4 mmol) was mixed in acetic acid (60 mL) and stirred further for 48 h at 90 °C. The mixture was

cooled down and mixed with 300 mL of water to obtain orange precipitate which is then filtered, washed with water, and dissolved in chloroform. After removal of chloroform by drying in $MgSO_4$, the precipitate (dimethyl 5-((2,4-dimethylphenyl)diazenylisophthalate) was purified by column chromatography. Next, 0.5 g of it was dissolved in 30 mL solution of THF, MeOH and 20% KOH (1:1:1), and stirred at 50 °C overnight. After the removal of organic phase, the aqueous phase was acidified with 6 M HCl to obtain yellow precipitate as ligand. Yield (2 %, 0.42 g). ^{1}H NMR (400 MHz, $CDCl_3$): δ 2.36 (s, 3H); 2.67 (s, 3H); 7.19 (d, 1H); 7.30 (s, 1H); 7.61 (d, 1H); 8.54 (d, 2H); 8.58 (t, 1H). FTIR (cm^{-1}): 2970, 2679, 2559, 1698, 1610, 1441, 1411, 1382, 1278, 1223, 1101, 1027, 917, 818, 763, 691, 667.

Synthesis of the PMOP

The synthesis of PMOP was carried out by following a procedure in our earlier report.[34] A $Cu_2(OAc)_4$•$2H_2O$ solution (120 mg, 0.3 mmol in 20 mL of DMA) was added in a DMA solution (10 mL) of 5-((2,4-dimethylphenyl)diazenyl)isophthalic acid (90 mg, 0.3 mmol) confined in vial and kept in dark for two days. Afterward, methanol (MeOH, 30 mL) was added to the solution to obtain a green precipitate, PMOP which is further washed with MeOH (three times) and kept in chloroform prior to use. FTIR (cm^{-1}): 3423, 2927, 1633, 1442, 1409, 1366, 1231, 1105, 1034, 924, 816, 778, 724, 664.

Synthesis of the ionic liquid (IL)

The IL, [PEG-linked bis(imidazoliumbutyl) di(trifluoromethanesulfonyl)amide, IL(NTf_2)] was synthesized in three steps. First, a biphasic system was formed by dissolving PEG-400 (1 M, 10 g) in a mixture of THF (25 mL) and 2.5 M aqueous solution of NaOH (2.5 g). Next, TOCl (1.1 M, 10.48 g) was added to this mixture while incubating in ice bath. Then, 1 M HCl (1.06 mL) was added to the reaction system at room temperature for 4 h. The product was extracted using DCM and water, and the solvent was removed using vacuum evaporation to obtain PEG-400-ditosylate which is later dissolved in a mixture of THF (25 mL) and 3 M aqueous solution of NaOH (3 g). Afterward, 2.2 M (7.5 g) of imidazole was added in the mixture and stirred at 80 °C for 4 h. In order to remove impurity from the resulting material, DCM and water were used, and then filtered. The product (PEG-functionalized bis-imidazole) was dried using vacuum evaporator to remove THF and DCM to obtain a viscous liquid. Second, in a round bottom flask, butyl bromide (16.5 mL) and PEG-linked bis-imidazole (8.2 mL) were added in dry toluene (20 mL), and kept on reflux under N_2 atmosphere at 80 °C for 24 h in a dark condition. This biphasic liquid medium was separated and the bottom fraction was washed with MeOH which is removed using vacuum evaporator to obtain a viscous product [PEG-linked bis(imidazolium butyl) di(trifluoromethanesulfonyl)amide, IL(Br)]. Third, to exchange the anion (Br^-), IL-Br (8.2 mL) and $LiNTf_2$ were dissolved in MeOH:H_2O (4:1) solution and stirred at room temperature for 4 h. The obtained material was washed with water and EtOAc twice, and separated using separating funnel while EtOAc was removed by vacuum evaporation to obtain pale yellow liquid [PEG-linked bis(imidazoliumbutyl) di(trifluoromethanesulfonyl)amide, IL(NTf_2)].Yield (5 %, 6.1 mL). ^{1}H NMR (400 MHz, DMSO-d_6): δ 0.91 (t, 3H); 1.28 (m, 2H); 1.79 (m, 2H); 3.51 (s, 8H); 3.79 (t, 2H); 4.20 (t, 2H); 4.35 (t, 2H); 7.76 (d, 1H); 7.79 (d, 1H); 9.13 (s, 1H). ^{13}C NMR (100 MHz, DMSO-d_6): δ 13.61,

19.23, 31.72, 49.07, 60.19, 70.21, 122.89, 123.29, 136.79 and 170.78. FTIR (cm^{-1}): 3153, 2951, 1567, 1462, 1353, 1194, 1133, 1051, 941, 792, 732.

Synthesis of the photoresponsive porous ionic liquids (PPILs)

A parent PPIL was prepared by dispersing PMOP (20 mg) in the solution of IL(NTf_2) (1 mL) and MeOH (1 mL), and ultra-sonicated for 20 min. Then, the resulting colloidal solution was dried at 70 °C for 1 h to obtain type III PPIL-2%. Next, to obtain the PPIL with PMOP contents 0.2, 0.1 and 0.05%, the parent PPIL-2% was diluted with IL(NTf_2) and MeOH accordingly, and ultra-sonicated for 20 min. These solutions were further kept in over at 70 °C for 2 h to remove MeOH so as to obtain lucid type II PPIL-0.2, 0.1 and 0.05%. Note: MeOH was used to lower the viscosity of IL(NTf_2) so that PMOP could be dispersed properly under sonication.

Gas adsorption measurements

Gas uptake analyses were measured on ASAP 2020 analyzer for low pressure adsorption (0 – 1 bar). CO_2 adsorption isotherms at 273 K were detected in an ice-water bath and after degas, the liquid samples in the quartz tube were irradiated with UV (365 nm) and Visible light (450 nm) using a xenon lamp (CEL-HXUV300) outfitted with a filter. For high pressure adsorption under UV and Visible light irradiations, BELSORP-HP instrument was employed within the pressure range of 0 – 10 bar at 25 °C. Prior to analyses; the liquid samples were evacuated at 100 °C for at least 2 h.

Simulation studies

Molecular dynamics simulations were conducted using the Forcite module in Accelrys Materials Studio 7.0 software.[38] The initial configuration was constructed with one photoresponsive metal-organic polyhedron (PMOP) cluster and one cation and two anions of the ionic liquid packed in a cubic box. The simulations were carried out by implementing Universal force field (UFF)[2] along with charge equilibration method (Q_{eq}) addressing point charges of the system. The calculation details are as follows: NPT ensembles with fixed pressure (100 kPa) and temperature (25 °C) were selected to conduct the equilibrium run for both systems (PMOPs with *cis* and *trans* structures), where the time step and total equilibrium time-run were set as 1.0 fs and 50 ns, respectively. Two simulated cubic boxes (28.565 and 28.585 Å) were obtained for *trans-* and *cis-* cages, respectively. The final configurations of the equilibrium run were retaken as the initial models for the production run under NVT conditions, where the time step and total equilibrium time-run were set as 1.0 fs and 25 ns, respectively. Radial distribution functions analysis was performed for the final confirmation of the production run. For all the dynamic calculations, a cut off distance of 15.5 Å were applied to both van der Waals and electrostatic potential. For each computed frame within the production run, movies were generated to interpret the movements of the studied models. Topological analysis tool Zeo++[3] was used to compute the pore size distribution map to distinguish the cavity space of the optimized configurations. A probe size of 0.5 Å and 100000 Monte Carlo cycles was implemented.

Data availability

All relevant data supporting the findings of this study are available from the corresponding authors on request.

Declarations

Acknowledgements

This work was supported by the National Science Fund for Distinguished Young Scholars (22125804) and the National Natural Science Foundation of China (22078155 and 21878149) and the Project of Priority Academic Program Development of Jiangsu Higher Education Institutions.

Author contributions

L.-B.S. and M.K.D conceived the research and designed the experiments. M.K.D and K.Z carried out the experimental part regarding IL and PPILs preparation, Z.D. conducted the high-pressure gas adsorption, L.D. performed the computational and molecular simulation studies, X.-Q.L and L.-B.S led the project overall. L.-B.S. and M.K.D are responsible for the major part of writing this paper, while all of the authors discussed the results and commented on the various versions of the paper.

Additional information

Supplementary Information accompanies this paper at http://www.nature.com/naturecommunications

Competing interests

The authors declare no competing interests.

References

1. Giri, N. et al. Liquids with permanent porosity. Nature **527**, 216–220 (2015).
2. Liu, H. et al. A hybrid absorption-adsorption method to efficiently capture carbon. Nat. Commun. **5**, 5147 (2014).
3. O'Reilly, N., Giri, N. & James, S. L. Porous liquids. Chem. – Eur. J. **13**, 3020–3025 (2007).
4. Bennett, T. D., Coudert, F. X., James, S. L. & Cooper, A. I. The changing state of porous materials. Nat. Mater. **20**, 1179–1187 (2021).
5. S. L. James. The dam bursts for porous liquids. Adv. Mater. **28**, 5712–5716 (2016).
6. Fulvio, P. F. & Dai, S. Porous liquids: the next frontier. Chem **6**, 3263–3287 (2020).
7. Jie, K., Zhou, Y., Ryan, H. P., Dai, S. & Nitschke, J. R. Engineering permanent porosity into liquids. Adv. Mater. **33**, 2005745 (2021).

8. Ma, L. et al. Coordination cages as permanently porous ionic liquids. Nat. Chem. **12**, 270–275 (2020).
9. Jie, K. et al. Transforming porous organic cages into porous ionic liquids via a supramolecular complexation strategy. Angew. Chem. Int. Ed. **59**, 2268–2272 (2020).
10. Knebel, A. et al. Solution processable metal–organic frameworks for mixed matrix membranes using porous liquids. Nat. Mater. **19**, 1346–1353 (2020).
11. Zhang, J. et al. Porous liquids: a promising class of media for gas separation. Angew. Chem. Int. Ed. **54**, 932–936 (2015).
12. He, S. et al. General way to construct micro- and mesoporous metal-organic framework-based porous liquids. J. Am. Chem. Soc. **141**, 19708–19714 (2019).
13. Shan, W. et al. New class of type III porous liquids: a promising platform for rational adjustment of gas sorption behavior. ACS Appl. Mater. Interfaces **10**, 32–36 (2018).
14. Greenaway, R. L. et al. Understanding gas capacity, guest selectivity, and diffusion in porous liquids. Chem. Sci. **8**, 2640–2651 (2017).
15. Egleston, B. D. et al. Controlling gas selectivity in molecular porous liquids by tuning the cage window size. Angew. Chem. Int. Ed. **59**, 7362–7366 (2020).
16. Wei, S. C. et al. A multistimuli-responsive photochromic metal-organic gel. Adv. Mater. **26**, 2072–2077 (2014).
17. Wieme, J., Lejaeghere, K., Kresse, G. & Speybroeck, V. V. Tuning the balance between dispersion and entropy to design temperature-responsive metal-organic frameworks. Nat. Commun. **9**, 4899 (2018).
18. Tang, J. H. et al. Temperature-responsive fluorescent organoplatinum(II) metallacycles. J. Am. Chem. Soc. **140**, 7723–7729 (2018).
19. Shivanna, M., Yang, Q. Y., Bajpai, A., Kazmierczak, E. P. & Zaworotko, M. J. A dynamic and multi-responsive porous flexible metal-organic material. Nat. Commun. **9**, 3080 (2018).
20. Qian, X. et al. Artificial phototropism for omnidirectional tracking and harvesting of light. Nat. Nanotech. **14**, 1048–1055 (2019).
21. Zheng, Y. et al. Flexible interlocked porous frameworks allow quantitative photoisomerization in a crystalline solid. Nat. Commun. **8**, 100 (2017).
22. Huang, N., Ding, X., Kim, J., Ihee, H. & Jiang, D. A photoresponsive smart covalent organic framework. Angew. Chem. Int. Ed. **54**, 8704–8707 (2015).
23. Haldar, R., Heinke, L. & Woll, C. Advanced photoresponsive materials using the metal-organic framework approach. Adv. Mater. **32**, 1905227 (2019).
24. Gu, Y. et al. Photoswitching topology in polymer network with metal-organic cages as crosslinks. Nature **560**, 65–69 (2018).
25. Fujiwara, H. & Yonezawa, Y. Photoelectric response of a black lipid membrane containing an amphiphilic azobenzene derivative. Nature **351**, 724–726 (1991).

26. Tan, E. M. M. et al. Fast photodynamics of azobenzene probed by scanning excited-state potential energy surfaces using slow spectroscopy. Nat. Commun. **6**, 5860 (2015).
27. Fregoni, J., Granucci, G., Coccia, E., Persico, M. & Corni, S. Manipulating azobenzene photoisomerization through strong light-molcule coupling. Nat. Commun. **9**, 4688 (2018).
28. Murase, T., Sato, S. & Fujita, M. Switching the interior hydrophobicity of a self-assembled spherical complex through the photoisomerization of confined azobenzene chromophores. Angew. Chem. Int. Ed. **46**, 5133–5136 (2007).
29. Baroncini, M. et al. Photoinduced reversible switching of porosity in molecular crystals based on star-shaped azobenzene tetramers. Nat. Chem. **7**, 634–640 (2015).
30. Dobbelin, M. et al. Light-enhanced liquid-phase exfoliation and current photoswitching in graphene-azobenzene composites. Nat. Commun. **7**, 11090 (2016).
31. Zhou, H. et al. Photoswitching of glass transition temperatures of azobenzene-containing polymers induces reversible solid-to-liquid transitions. Nat. Chem. **9**, 145–151 (2017).
32. Jiang, Y. et al. Metal-organic frameworks with target-specific active sites switched by photoresponsive motifs: efficient adsorbents for tailorable CO_2 capture. Angew. Chem. Int. Ed. **58**, 6600–6604 (2019).
33. Park, J., Sun, L. B., Chen, Y. P., Perry, Z. & Zhou, H. C. Azobenzene-functionalized metal-organic polyhedra for the optically responsive capture and release of guest molecules. Angew. Chem. Int. Ed. **53**, 5842–5846 (2014).
34. Jiang, Y. et al. Maximizing photoresponsive efficiency by isolating metal-organic polyhedra into confined nanoscaled spaces. J. Am. Chem. Soc. **141**, 8221–8227 (2019).
35. Gomes, M. C., Pison, L., Cervinka, C. & Padua, A. Porous ionic liquid or liquid metal-organic frameworks? Angew. Chem. Int. Ed. **57**, 11909–11912 (2018).
36. Zhao, H. et al. Designing enzyme-compatible ionic liquids that can dissolve carbohydrates. Green Chem. **10**, 696–705 (2008).
37. Tang, S., Baker, G. A., Ravula, S., Jones, J. E. & Zhao, H. PEG-functionalized ionic liquids for cellulose dissolution and saccharification. Green. Chem. **14**, 2922–2932 (2012).
38. Rappé, A. K. et al. UFF, a full periodic table force field for molecular mechanics and molecular dynamics simulations. J. Am. Chem. Soc. **114**, 10024–10035 (1992).

Figures

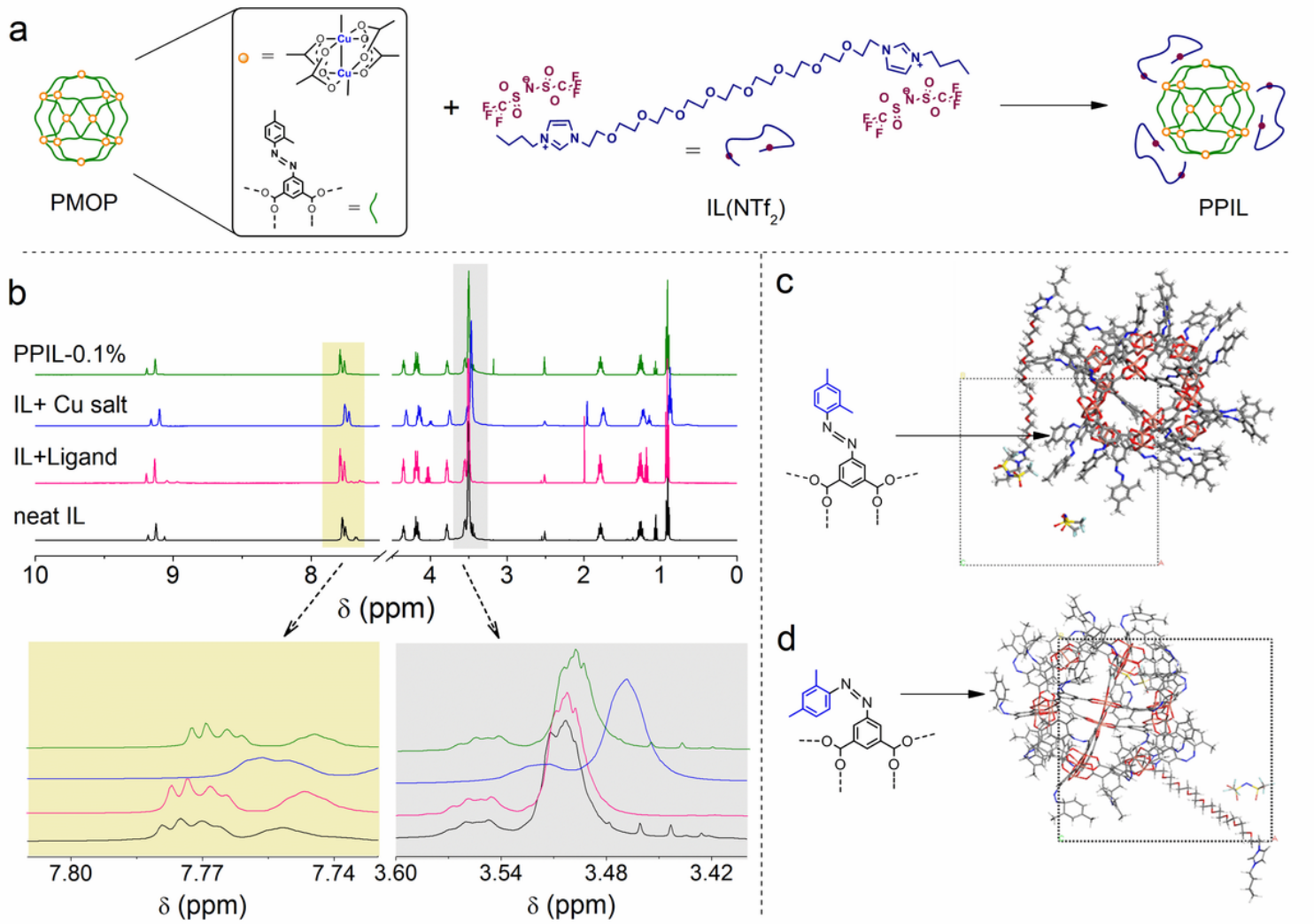

Figure 1

Construction of PPILs. a Scheme depicting the preparation of type II PPIL by solubilizing PMOP in size-excluded IL(NTf_2) [Insets are the 'orange dot' and 'green strand' representing copper paddle wheel and organic moiety in PMOP]. **b** ^1H NMR spectra depicting downward shifts (d) in PPIL than neat IL due to the magnetic susceptibility of Cu-based complexes (PMOP) in IL. This is exemplified by adding $Cu(OAc)_2$ in the neat IL(NTf_2) (IL + Cu salt). Notably, mere the existence of ligand in IL (IL + ligand) depicted no shifts (d) in the peaks. **c** and **d** Molecular dynamic simulations for confirming the bulkiness of IL molecule against *trans*- and *cis*-PMOP in a box.

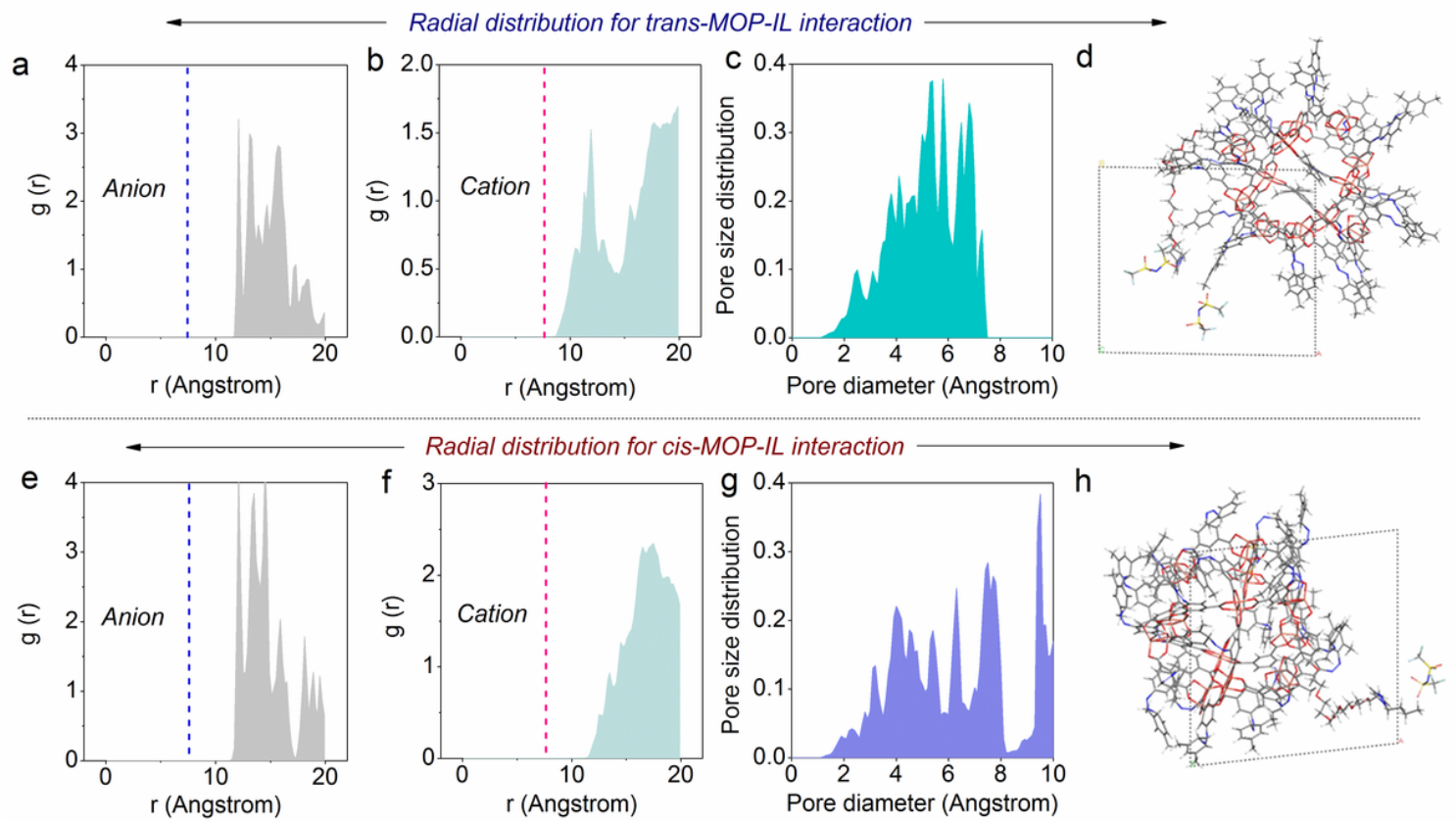

Figure 2

Radial distribution functions correlated with the centroid of the cages and ionic liquid. **a** and **e** Set of anion. **b** and **f** Set of cation (dash line stands for the largest diameter inter-cavity sphere). **c** and **g** Pore size distribution functions. **d** and **h** Optimized final configurations for the interaction of ionic liquid molecule with *trans*- and *cis*-MOP.

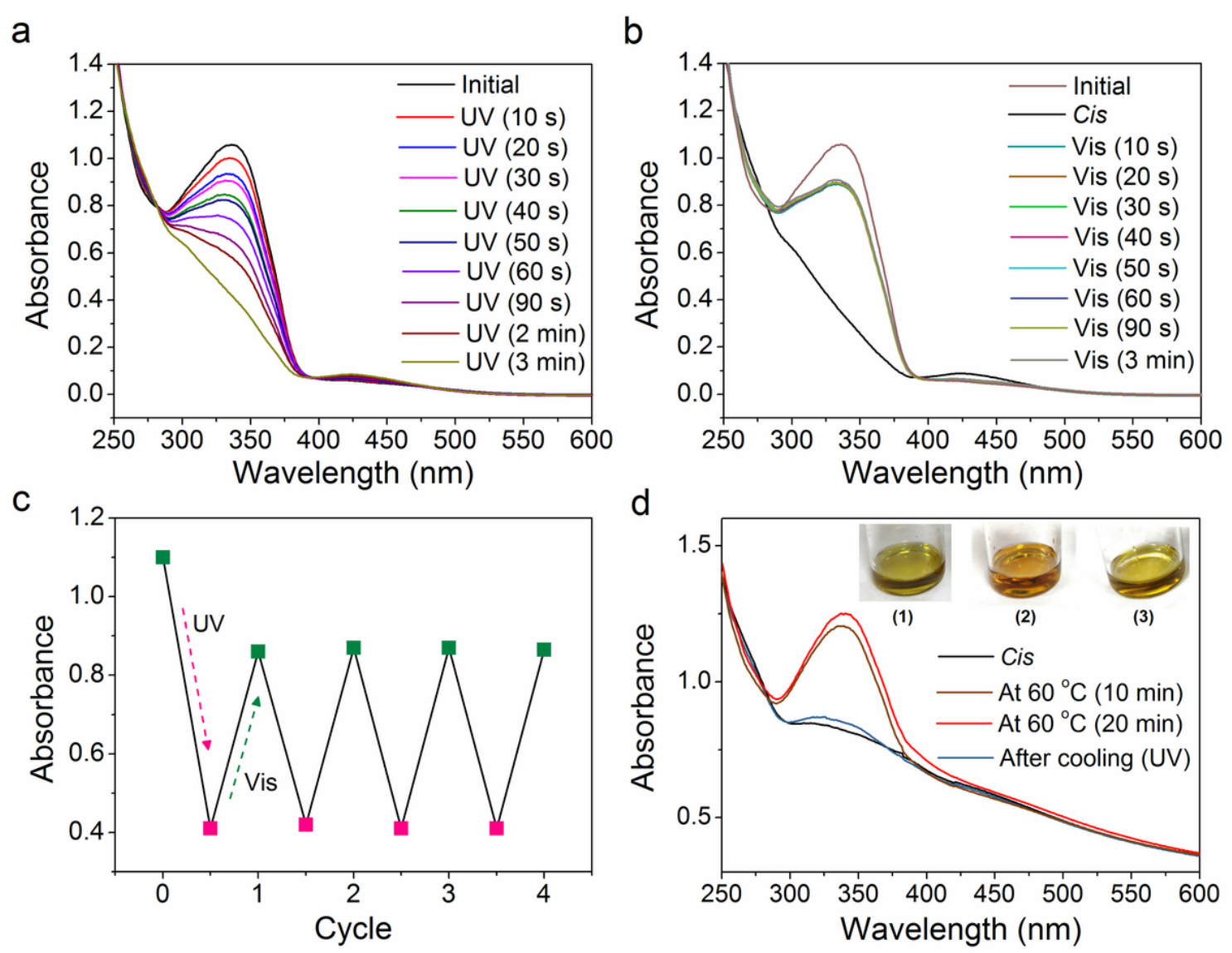

Figure 3

Stimuli response of PPILs. a and **b** *cis*- and *trans*-isomerization of PPIL-0.1% under consecutive UV (365 nm) and visible light (450 nm) irradiations. **c** Four successive reversible isomerization of PPIL-0.1% by switching UV and visible lights. **d** *cis*- to *trans*-isomerization of PPIL-0.2% after heating in dark [Inset is the sample of PPIL-0.2% (1) before and (2) after heating as well as (3) after cooling down].

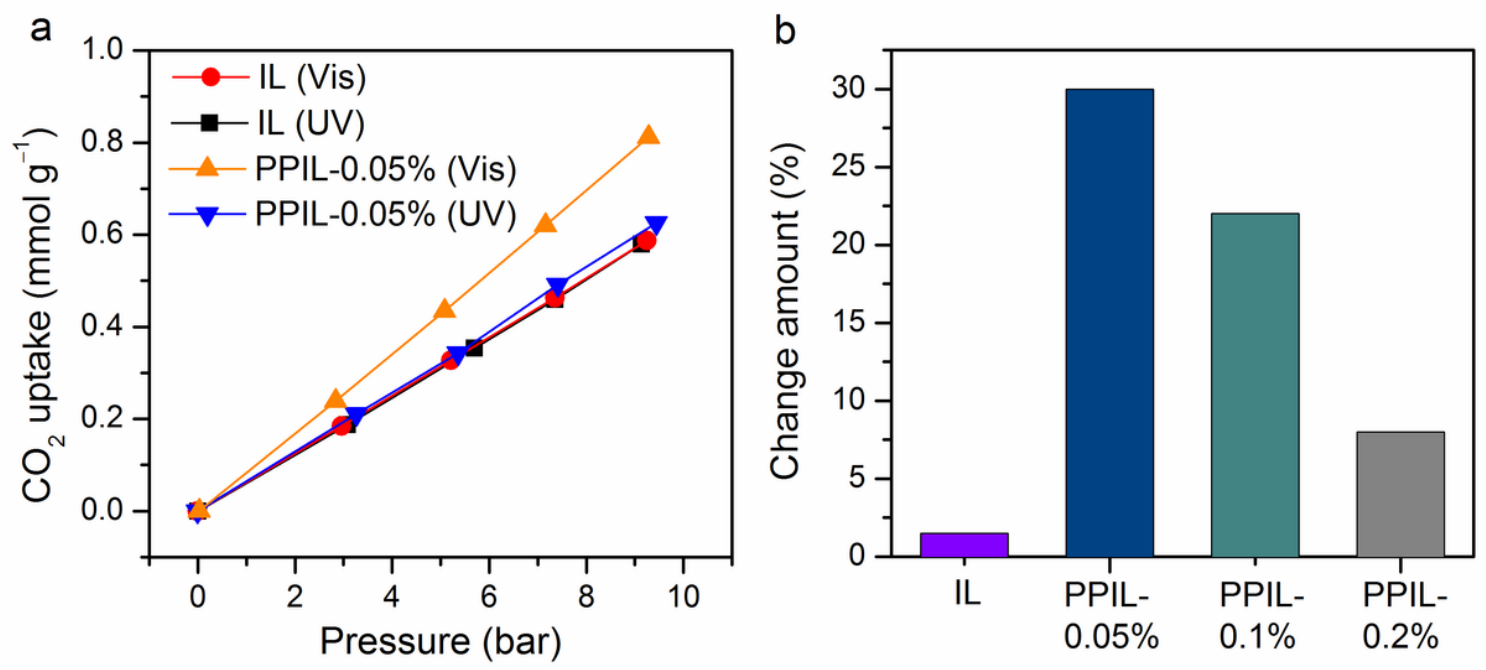

Figure 4

Controlled guest uptakes under light irradiation. a CO_2 interaction behaviors at high pressure under visible (450 nm) and UV light (365 nm) irradiations using PPIL and IL. **b** Changes in CO_2 uptake (at 10 bar, 25 °C) by PPILs and IL upon visible and UV light irradiations.

Supplementary Files

This is a list of supplementary files associated with this preprint. Click to download.

- NCPPILsrevisedSuppInfo.pdf
- VideoS1.mp4
- VideoS2.mp4